Compton Profile Study of Aluminium Nitride

Vimal Vyas^a, Yogesh Chandra Sharma^a, Vinod Purvia^a, Narayan Lal Heda^b, Yamini Sharma^c, Babu Lal Ahuja^b, and Bal Krishna Sharma^a

^a Department of Physics, University of Rajasthan, Jaipur-302004, Rajasthan, India

^c Department of Physics, Feroze Gandhi College, Rae Bareli-229001, U. P., India

Reprint requests to Prof. B. L. A.; E-mail: blahuja@yahoo.com

Z. Naturforsch. 62a, 703 – 710 (2007); received May 30, 2007

In this paper we report the *ab-initio* theoretical Compton profiles of aluminium nitride (AlN) in the framework of the Hartree-Fock, density functional theory and hybridization of Hartree-Fock to density functional theories using the CRYSTAL03 code. To compare our first ever theoretical data, we have also measured the isotropic Compton profile of AlN, using 59.54 keV γ -rays. The Hartree-Fock scheme-based Compton profile agrees better with the experiment than the other theories. The energy bands, density of states and Mulliken's population analysis, using the CRYSTAL03 code, are also reported. Our band structure calculations show a large band gap, while Mulliken's population analysis shows the ionic nature of bonding in AlN.

Key words: X-Ray Scattering; Band Structure Calculation; Density Functional Theory; III-V Semiconductor.

PACS numbers: 13.60.Fz, 71.15.Ap, 71.15.Mb, 78.70.-g

1. Introduction

Compton spectroscopy is a powerful and sensitive experimental tool for studying the electron momentum distribution in materials [1,2]. Using this technique the chemical properties can be correlated with the electronic structure through the electron momentum density $n(\vec{p})$.

The measured one-dimensional quantity, called Compton profile $J(p_z)$, is a projection of the three-dimensional momentum density $n(\vec{p})$ along the scattering vector parallel to p_z . Mathematically

$$J(p_z) = \int_{p_x} \int_{p_y} n(\vec{p}) dp_x dp_y, \qquad (1)$$

where p_z is the electron momentum along the z-direction, which is along the direction of the experimental scattering vector.

Aluminium nitride (AlN), a tetrahedrally coordinated III-V compound with a hexagonal wurtzite structure (space group $P6_3mc$), is of great technological importance due to its large band gap, high electrical resistivity, high thermal conductivity, large bulk modulus and piezoelectric behaviour.

Much experimental and theoretical work has been devoted to AlN due to its semiconducting and optical properties; see for example [3–17]. Recently a number of diverse bulk properties of III-V nitrides has been predicted from first principles within the density functional theory (DFT), using the plane wave ultrasoft pseudopotential method within both the local density approximation (LDA) and the generalized gradient approximation (GGA) [18]. Lepkowski et al. [19] studied the nonlinear elasticity effects in the wurtzite (WZ) crystallographic phase of AlN by performing *ab-initio* calculations in the framework of plane wave pseudopotential implementation of the DFT.

The DFT has been used effectively to explore structural and optical properties of III-nitrides in general, and AlN in particular. However, to our knowledge none of nitrides has been studied theoretically employing the DFT to derive the Compton profile, which play a peculiar role in examining the various theoretical models and is an important observable to unravel bonding and bands in solids. Therefore, first ever Compton profile calculations for AlN as a representative of III-nitrides have been undertaken in the present study.

In this paper we report Compton profiles, energy bands and density of states (DOS) using a self-con-

0932–0784 / 07 / 1200–0703 \$ 06.00 \odot 2007 Verlag der Zeitschrift für Naturforschung, Tübingen \cdot http://znaturforsch.com

^b Department of Physics, University College of Science, M. L. Sukhadia University, Udiapur-313001, Rajasthan, India

sistent linear combination of atomic orbitals (LCAOs) calculation within the framework of Hartree-Fock (HF) and DFT schemes of the CRYSTAL03 code of the Torino group [20-22]. Besides this, using the free atom profile of Biggs et al. [23], we have calculated the Compton profiles within an ionic model $Al^{+x}N^{-x}$ (x varies from 0 to 3). Regarding Compton profile measurements on AlN, more than three decades ago Hosova et al. [24] have reported the Compton profile of polycrystalline AlN employing X-rays. This measurement has limitations due to the low input energy of X-ray photons, X-ray doublets, uncertainties in removing the background, limitations of data analysis, etc. To compare our theory, we have also measured an accurate isotropic Compton profile of AlN. The isotropic measurement was made because of nonavailability of large size (13 mm diameter and 2 mm thickness) single crystals of AlN.

The paper is organized as follows: Experiment and data analysis are given in Section 2. A brief description of the LCAO and ionic model calculations is given in Section 3. Results and discussion are presented in Section 4, while conclusions are given in Section 5.

2. Experimental and Data Analysis

In the present measurement, the γ -ray Compton spectrometer with an annular 5 Ci ²⁴¹Am source described by Sharma et al. [25] has been used. The polycrystalline sheet of 25 mm × 25 mm cross-section and 0.64 mm thickness (purity 99.5%) was held vertically in the scattering chamber. The chamber was evacuated to about 1.3 Pa to reduce the contribution of air scattering. The γ -rays of 59.54 keV were allowed to scatter by the sample through a mean angle of $(167 \pm 2.5)^{\circ}$. The scattered photons were detected and analysed using a high purity Ge detector (Canberra model, GL0110P), which was cooled to liquid nitrogen temperature. The overall momentum resolution of the Compton spectrometer was Gaussian with full width at half maximum (FWHM) of 0.55 a.u. The spectrum was collected in a multi-channel analyzer (MCA) with 4096 channels having a channel width of 20 eV, which corresponds to about 0.03 a. u. During the exposure time of 30 h about 60,000 counts were collected at the Compton peak. During the measurements, the stability of the electronic system was checked from time to time by a weak ²⁴¹Am calibration source. The background was measured separately and then subtracted from the above data point by point after scaling it to the counting time for the sample. Then, the measured profile was corrected for the effects of the detector response function, energy-dependent absorption and scattering cross-section, according to the scheme described by the Warwick group [2, 26]. The data reduction for the detector response function was restricted to stripping the low energy tail off the resolution function and smoothing the data, leaving the theory to be convoluted with a FWHM of 0.55 a. u. After converting the profile to the momentum scale, a Monte Carlo simulation of the multiple scattering was performed. Finally, the experimental Compton profile was normalized to 9.63 electrons being the area of the free atom profile [23] in the momentum range 0 to +7.0 a. u.

3. Theoretical Calculations

3.1. LCAO Calculations

Compton profiles of AlN have been computed in the LCAO scheme using HF and DFT methods of the CRYSTAL03 code [20–22]. The electron density within Kohn-Sham (KS) (DFT) and HF approximations can be written as

$$n_{\text{KS/HF}}(\vec{r}) = \int_{BZ} d\vec{k} \sum_{j=occ} \left| \phi_{j,\text{KS/HF}}^{k}(\vec{r}) \right|^{2}, \qquad (2)$$

where the crystalline orbitals $\phi_{j, \text{KS/HF}}^{k}$ are the solution of

$$\hat{h}_{\text{KS/HF}} \phi_{j,\text{KS/HF}}^k(\vec{r}) = \varepsilon_{j,\text{KS/HF}}^k \phi_{j,\text{KS/HF}}^k(\vec{r}). \tag{3}$$

Here $\varepsilon_{j,\text{KS/HF}}^k$ are the one-electron energies corresponding to $\phi_{j,\text{KS/HF}}^k$.

The one-electron Hamiltonian operator, $\hat{h}_{\rm HF}$, in the HF approach is given by

$$\hat{h}_{HF} = \hat{T} + \hat{V} + \hat{J}[n(\vec{r})] + \hat{K}[n(\vec{r}, \vec{r}')], \tag{4}$$

where \hat{T} , \hat{V} , \hat{J} and \hat{K} are the kinetic, external potential, Coulomb and exchange operators, respectively. In the HF operator, the exact exchange interaction between electrons is taken care of. In the DFT, the HF Hamiltonian operator is replaced by the Kohn-Sham monoelectron operator as

$$\hat{h}_{KS} = \hat{T} + \hat{V} + \hat{J}[n(\vec{r})] + \hat{v}_{XC}(\vec{r}).$$
 (5)

The exchange-correlation potential operator $\hat{v}_{XC}(\vec{r})$ in the DFT is given as

$$\hat{\mathbf{v}}_{\mathrm{XC}} = \frac{\partial E_{\mathrm{XC}}[n(\vec{r})]}{\partial n(\vec{r})},\tag{6}$$

where $E_{\rm XC}$ is the exchange-correlation density functional energy and $n(\vec{r})$ is the charge density at a point r. In the LDA and GGA, $E_{\rm XC}$ is defined as

$$E_{\rm XC}^{\rm LDA}[n(\vec{r})] = \int n(\vec{r}) \varepsilon_{\rm XC}[n(\vec{r})] d\vec{r}, \tag{7}$$

$$E_{\text{XC}}^{\text{GGA}}[n(\vec{r})] = \int n(\vec{r}) \varepsilon_{\text{XC}}[n(\vec{r}), |\nabla n(\vec{r})|] d\vec{r}, \quad (8)$$

where $\varepsilon_{\rm XC}$ is the exchange-correlation energy per particle in a uniform electron gas. Further, within the notations of CRYSTAL03 [20], $n(\vec{r})$ can also be written as

$$n_{\text{KS/HF}}(\vec{r}) = \sum_{\mu,\nu,g} P_{\text{KS/HF}}^{\mu,\nu,g} \chi_{\mu}(\vec{r}) \chi_{\nu}(\vec{r}),$$
 (9)

where $\chi_{\mu}(\vec{r})$ and $\chi_{\nu}(\vec{r})$ are atomic orbitals, respectively, associated with the $o^{\rm th}$ and $g^{\rm th}$ cells of the LCAO periodic HF or KS methods and $P_{\rm KS/HF}^{\mu,\nu,g}$ are the corresponding density matrix elements.

In the momentum space, the electron momentum density can be calculated as

$$n_{\text{KS/HF}}(\vec{p}) = \sum_{\mu,\nu,g} P_{\text{KS/HF}}^{\mu,\nu,g} \chi_{\mu}(\vec{p}) \chi_{\nu}(\vec{p}), \tag{10}$$

where
$$\chi(\vec{p}) = \int \chi(\vec{r}) e^{-i\vec{p}\cdot\vec{r}} d\vec{r}$$
.

In the DFT-LDA we have chosen the Dirac-Slater exchange as given in [22] and the Perdew-Zunger [27] correlation functionals, whereas for DFT-GGA we have used the exchange functional of Becke [28] and the correlation functional of Perdew and Wang [29]. Following recent attempts of splitting the exchange and correlation contributions [30], we have also performed calculations using the B3LYP scheme. In the B3LYP, $E_{\rm XC}$ is defined as

$$\begin{split} E_{\rm XC} &= 0.80 \cdot \left(E_{\rm X}^{\rm LDA} + 0.90 \cdot \Delta E_{\rm X}^{\rm BECKE} \right) \\ &+ 0.20 \cdot E_{\rm X}^{\rm HF} + 0.19 \cdot E_{\rm C}^{\rm VWN} + 0.81 \cdot E_{\rm C}^{\rm LYP}. \end{split} \tag{11}$$

 $E_{\rm X}^{\rm HF}$ and $E_{\rm X}^{\rm LDA}$ are the exchange energies of HF and Dirac-Slater, respectively. $\Delta E_{\rm X}^{\rm BECKE}$ is Becke's gradient correction to the exchange functional, while $E_{\rm C}^{\rm VWN}$ and $E_{\rm C}^{\rm LYP}$ are the correlation energies of Vosko-Wilk-Nusair [31] and Lee-Yang-Parr [32], respectively.

Therefore, the B3LYP functional is a hybrid of the exact (HF) exchange with local and gradient-corrected exchange and correlation terms, as first suggested by Becke [33]. The standard prefactors, with which different weightage for exchange and correlation energies

enter in (11), were also suggested by Becke [33]. These prefactors were based on fitting to heats of formation of molecules. In the B3LYP functional the values of the prefactors are taken as such along with LYP for the correlation functional.

In the present calculations, the all-electron basis sets of Gaussian-type orbitals (GTOs) for Al and N have been adopted after optimization, using BILLY software [20]. The all-electron basis sets of Al (85-11G*) and for N (7-311G) are taken from [34]. The optimization has been performed for the WZ structure of AlN with the lattice parameters a=3.111~Å and c=4.978~Å [35]. The integration in the reciprocal space has been carried out on a grid of 133 \vec{k} points in the irreducible Brillouin zone.

3.2. Ionic Model

The theoretical Compton profiles of AlN for different ionic configurations were calculated from the free atom profiles of Al and N as taken from Biggs et al. [23]. The valence profiles for various $Al^{+x}N^{-x}$ (x varies from 0 to 3) configurations were calculated by transferring x electrons from the 3p and 3s shell of Al to the 2p shell of N.

For $A^N B^{8-N}$ materials like AlN, the valence profile was normalized to four electrons in the momentum range 0-7 a. u. and was added to the free atom core contributions [23], to get the total profiles. In the case of HF and DFT calculations, the core profiles generated by the CRYSTAL03 code were used. All profiles were then normalized to 9.63 electrons, as described earlier.

4. Results and Discussion

In Figs. 1 and 2, we have plotted the energy bands and corresponding DOS using DFT-LDA and B3LYP schemes in the energy range -0.75 to +0.50 Hartree. Since the band dispersions in case of the DFT-GGA were almost identical to the DFT-LDA, we have not shown the bands corresponding to DFT-GGA scheme. The Fermi energy $E_{\rm F}$ is shown using a horizontal solid line. The topology of our energy bands is found to agree with those given by Rubio et al. [36] and Armenta et al. [37]. The values of the band gap computed using DFT-LDA, DFT-GGA and B3LYP along with the available data [36–41] are listed in Table 1. The large band gaps computed using the DFT with LDA and GGA agree with the data reported by Stampfl

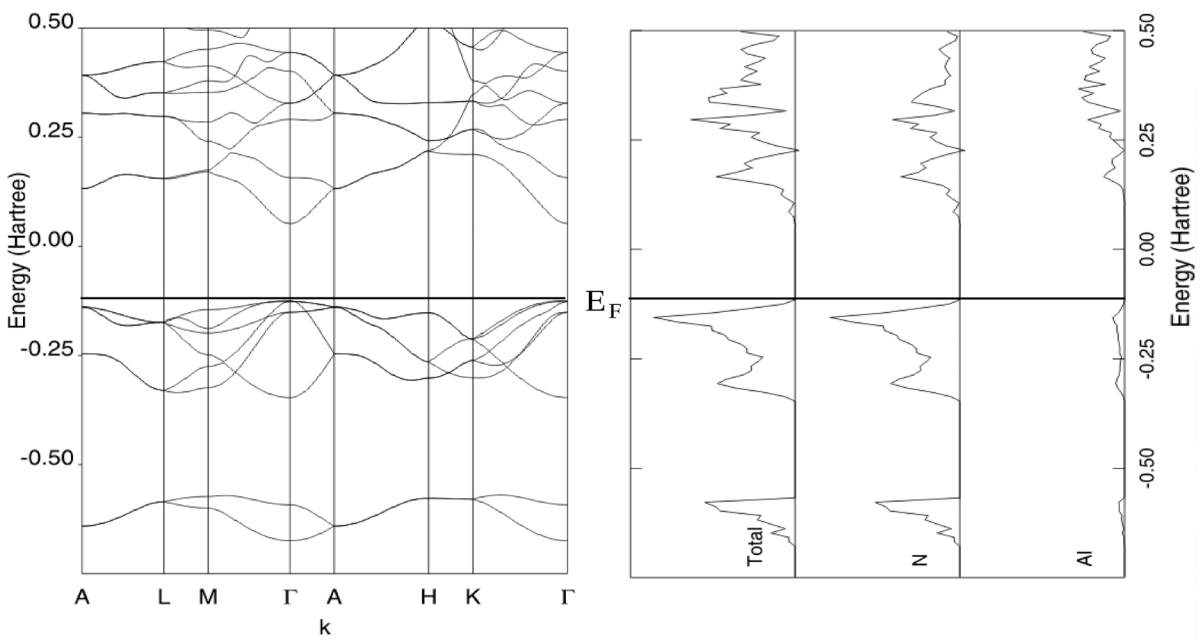


Fig. 1. Band structure (E-k relation) and density of states of wurtzite AlN along with high symmetry directions of the first Brillouin zone within DFT-LDA. The horizontal solid line corresponds to the Fermi energy. The band gap is calculated at Γ point. The positions of the A, L, M, Γ , A, H, K and Γ vertices correspond to (0, 0, 1/2), (1/2, 0, 1/2), (1/2, 0, 0), (0, 0, 0), (0, 0, 1/2), (1/3, 1/3, 1/2), (1/3, 1/3, 0) and (0, 0, 0). One Hartree is equal to 27.212 eV.

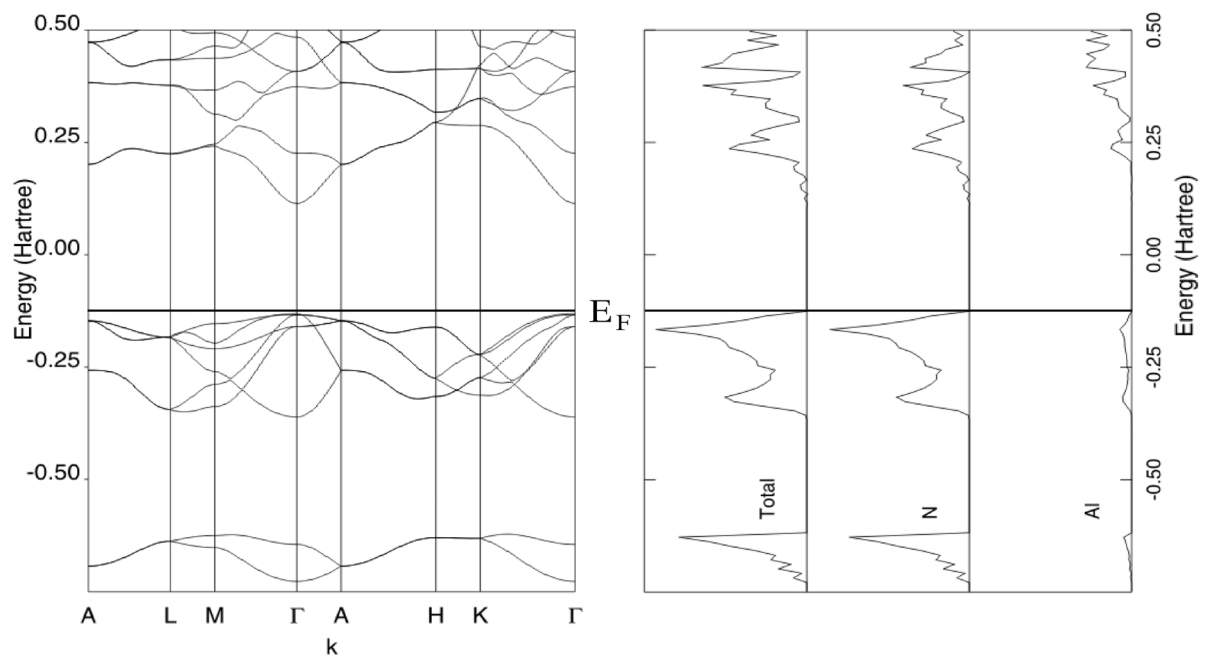


Fig. 2. Same as in Fig. 1 except for the scheme, which is B3LYP.

and Van de Walle [38], in which the authors have used pseudopotential plane waves with LDA approach. The

band gap computed within B3LYP is close to the experimental band gap reported by Berger [39]. It is seen

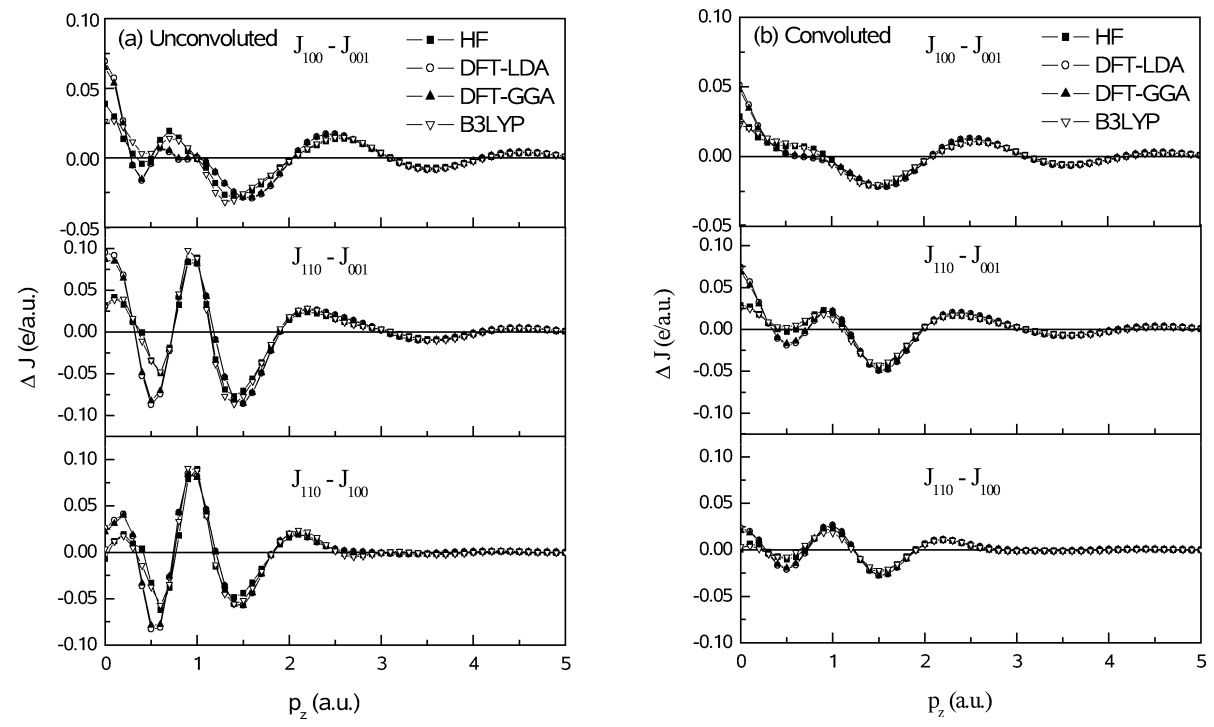


Fig. 3. Difference in the directional Compton profiles computed using various schemes of the CRYSTAL03 code for (a) unconvoluted and (b) convoluted with a representative Gaussian of FWHM 0.55 a.u. The solid lines connecting the symbols are drawn to guide the eyes.

	Band gap at Γ point 4.80
(i) Our work (a) DFT-LDA (b) DFT-GGA (c) B3LYP (ii) Rubio et al. [36]	
(a) DFT-LDA (b) DFT-GGA (c) B3LYP (ii) Rubio et al. [36]	4.80
(b) DFT-GGA (c) B3LYP (ii) Rubio et al. [36]	4.80
(c) B3LYP (ii) Rubio et al. [36]	
(ii) Rubio et al. [36]	4.77
	6.68
(a) I DA	
(u) LD/1	3.90
(b) GW	5.80
(iii) Armenta et al. [37]	
(a) $HF + PZB$ (6-21G)	5.47
(b) HF+ PZB (6-21 G*)	5.25
(iv) Pseudopotential [38]	4.74
(v) LCAO [40]	4.44
(vi) GDFT-LDA [41]	6.01
(vii) Experiment [39]	

Table 1. Band gap (in eV) of wurtzite AlN. One Hartree is equal to 27.212 eV.

from Table 1 that our DFT calculations overestimate the band gap in comparison to LCAO data reported by Ching and Harmon [40] and LDA data of Rubio et al. [36]. On the other hand, it is lower than the generalized DFT-LDA data of Remediakis and Kaxiras [41] and GW (G stands for Green function, while W stands for the screened Coulomb interaction) data of Rubio et al. [36]. In a separate calculation we have also cal-

culated the band gap using a pure HF scheme, which was found to be higher. This trend is consistent with the general observation that the HF calculation overestimates the band gap, while the DFT-LDA calculation underestimates it [42]. Except for some fine structures, the overall shape of the DOS in Figs. 1 and 2 is similar to an earlier work reported by Ching and Harmon [40].

A Mulliken population analysis within the DFT-LDA and DFT-GGA calculations shows the corresponding charge transfer of 2.29 and 2.32 electrons from Al to N. An overlap population of about 0.106 electrons between Al and N indicates the strong ionic nature of bonding in AlN. It may be noted that Mulliken's population is reliable in the present case, because the overlap population is relatively low and the external atomic orbitals of Al and N are not too diffuse. This is supported by the values of the exponents of the external basis set, which are 0.4409 and 0.5504 for Al and 0.4288 and 0.1302 for N. It is also seen that the charge transfer and overlap population from B3LYP are almost the same as from DFT-GGA.

In Fig. 3, we have plotted the unconvoluted and convoluted anisotropies between the theoretical Compton

Table 2. The unconvoluted spherically averaged theoretical Compton profiles (HF, DFT with LDA and GGA) of AlN as computed using CRYSTAL03 code. The B3LYP corresponds to hybridization of HF and DFT methods. The ionic Compton profiles (best agreed) along with experimental profiles are also listed. The statistical errors at a few points $(\pm \sigma)$ are also given.

p _z (a. u.)	$J(p_z)$ (e/a.u.)						
	HF	DFT-LDA	DFT-GGA	B3LYP	Ionic Al ^{+2.6} N ^{-2.6}	Experimental	
0.0	6.094	6.154	6.171	6.129	5.991	5.861 ± 0.014	
0.1	6.065	6.124	6.140	6.100	5.858	5.834	
0.2	5.975	6.030	6.045	6.010	5.674	5.748	
0.3	5.830	5.871	5.885	5.859	5.458	5.604	
0.4	5.626	5.654	5.666	5.647	5.217	5.407	
0.5	5.363	5.386	5.397	5.376	4.946	5.163	
0.6	5.048	5.067	5.075	5.053	4.650	4.879	
0.7	4.688	4.693	4.699	4.685	4.338	4.564	
0.8	4.288	4.273	4.275	4.278	4.021	4.226	
1.0	3.433	3.383	3.378	3.404	3.414	3.507 ± 0.011	
1.2	2.670	2.627	2.620	2.638	2.880	2.829	
1.4	2.148	2.124	2.118	2.130	2.434	2.299	
1.6	1.818	1.807	1.803	1.813	2.069	1.902	
1.8	1.581	1.579	1.577	1.582	1.774	1.630	
2.0	1.390	1.391	1.389	1.392	1.532	1.414 ± 0.007	
3.0	0.769	0.771	0.769	0.771	0.792	0.773 ± 0.005	
4.0	0.445	0.446	0.445	0.446	0.452	0.453 ± 0.004	
5.0	0.276	0.276	0.275	0.276	0.279	0.295 ± 0.003	
6.0	0.182	0.182	0.181	0.181	0.182	0.193 ± 0.002	
7.0	0.125	0.125	0.125	0.125	0.129	0.132 ± 0.002	

profiles. To see the effect of resolution in the measurement of anisotropies using a conventional ²⁴¹Am spectrometer like the present one, we have convoluted the theoretical profiles with a representative Gaussian function of FWHM 0.55 a.u. From Fig. 3a, it can be seen that the maximal anisotropy is between the [110] and [001] directions. The trend of anisotropies between [110] and [001] and also [110] and [100] is almost equal. A small amplitude of anisotropy between [100] and [001] can be explained on the basis of energy bands in the respective branches, namely Γ -M and Γ -A. Along the Γ -M direction, just below $E_{\rm F}$, there are many allowed states, while two degenerate states are seen at A point of the Γ -A branch. So both branches contribute almost a similar momentum density which roughly cancels J_{100} - J_{001} , leading to a small amplitude of the anisotropy. On the contrary, such a type of cancellation is absent in J_{110} - J_{001} and J_{110} - J_{100} . As depicted by Fig. 3b, the amplitude of differences derived from the convoluted theoretical profiles is lower than the unconvoluted profiles, which shows that in such experiments, with 0.55 a. u. resolution, the difference between LDA and GGA is hardly significant and is small with respect to HF also. Therefore, high resolution directional Compton profile measurements are needed to examine these calculations.

The unconvoluted spherically averaged theoretical Compton profiles (HF, DFT with LDA and GGA and B3LYP) and best-agreed ionic Compton profile of AlN along with experimental profiles are listed in Table 2. It is seen from Table 2 that there is a small difference between the DFT profiles computed within the LDA and GGA schemes.

In order to examine quantitatively the agreement of various theoretical profiles of AlN with the experiment, theoretical profiles have been convoluted with a Gaussian function of 0.55 a. u. to incorporate the instrumental smearing.

In Fig. 4, we show the difference curves in experimental and various theoretical Compton profiles together with experimental errors at a few points. All the theoretical profiles considered here include solid state effects, except the best ionic arrangement, and all are duly convoluted. The agreement between theory and experiment is very poor for the ionic model. It improves for CRYSTAL03-based theories.

Due to different kinds of exchange and correlation approximations in band calculations, these profiles differ on the low momentum side ($p_z \le 2$ a.u.). In the high momentum region ($p_z > 3$ a.u.), all the theoretical profiles are effectively the same, which is expected because the contribution from inner electrons is identical in all the calculations, and the Compton profile

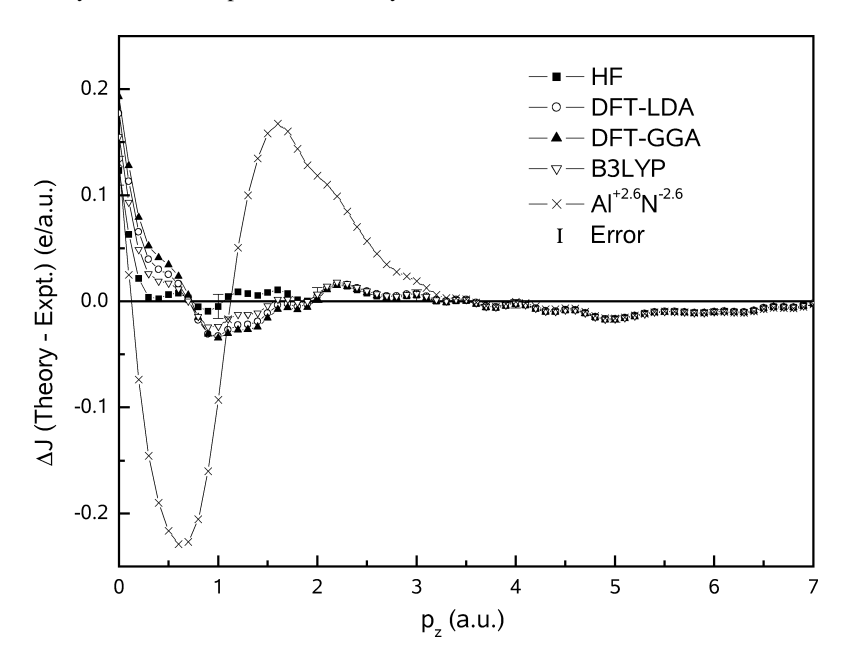


Fig. 4. Difference between the convoluted theoretical profiles (HF, DFT with LDA and GGA, B3LYP and best ionic model) and the isotropic experimental profile. The solid lines connecting the symbols are drawn to guide the eyes. Statistical error is shown for a few representative values.

contribution of the valence electrons is insignificant in this region. From Fig. 4 it can be judged that in the low momentum region the HF theory shows less deviation from the experimental data, in comparison to the DFT. On the basis of χ^2 tests and this figure, it is seen that the HF gives the best overall agreement amongst all the theories. It is worth mentioning here that such a trend has also been observed in our earlier data of II-VI semiconductors, namely ZnSe, CdS and CdTe [42], and a zero band gap semimetal, namely Sn [43]. The difference between theoretical and experimental profiles near $p_z = 0$ a. u. may be due to (a) limitations of a finite number of basis sets, (b) neglect of the correlation effect in the HF theory, and (c) approximate inclusion of exchange correlation effects in DFT.

5. Conclusions

In this paper, we have presented the results of a Compton scattering study of a III-V semiconductor, namely AlN. The measured isotropic Compton profile is compared with an ionic model and various schemes (Hartree-Fock and density functional theory) of the

Acknowledgement

along the principal directions.

The authors are grateful to the Department of Science and Technology (DST), New Delhi (India) for financial support through grant No. SP/S2/M45/99 and Govt. of India, New Delhi through grant No. 0303434M/01-DRDO. We are also grateful to Prof. R. Dovesi and the CRYSTAL Support Team for providing the CRYSTAL03 computer code.

CRYSTAL03 code. The present HF and DFT calcula-

tions deal with all electron Gaussians to describe accu-

rately the electronic distributions in both the valence

and core regions. The HF scheme has described the

electronic behaviour of AlN in a better way than the

DFT, in sharp contrast to the metals. The computed

energy bands agree with the available data and con-

firm the wide band gap of AlN. Mulliken's population

analysis shows a large charge transfer from Al to N,

which indicates the ionic nature of bonding in AlN.

All the inferences would seem to get strengthened with

the synchrotron-based high resolution measurements

- [1] M. J. Cooper, Rep. Prog. Phys. 48, 415 (1985).
- [2] B.G. Williams (Ed.), Compton Scattering, McGraw-Hill, London 1977; M.J. Cooper, P.E. Mijnarends, N. Shiotani, N. Sakai, and A. Bansil, X-Ray Comp-
- ton Scattering, Oxford Science Publications, New York
- [3] E. Gabe, Y. Le Page, and S. L. Mair, Phys. Rev. B 24, 5634 (1981).

- [4] K. Nakahigashi, H. Ishibashi, and S. Minamigawa, J. Phys. Chem. Solids 54, 445 (1993).
- [5] Q. Guo, M. Nishio, H. Ogawa, and A. Yoshida, Phys. Rev. B 64, 113105 (2001).
- [6] D. Fritsch, H. Schmidt, and M. Grundmann, Phys. Rev. B 67, 235205 (2003).
- [7] E. Ruiz, S. Alvarez, and P. Alemany, Phys. Rev. B 49, 7115 (1994).
- [8] N.E. Christensen and I. Gorczyca, Phys. Rev. B 47, 4307 (1993).
- [9] N.E. Christensen and I. Gorczyca, Phys. Rev. B 50, 4397 (1994).
- [10] A. K. Solanki, A. Kashyap, T. Nautiyal, S. Auluck, and M. A. Khan, Solid State Commun. 94, 1009 (1995).
- [11] K. Miwa and A. Fukumoto, Phys. Rev. B 48, 7897 (1993).
- [12] G. A. Jeffrey, G. S. Parry, and R. L. Mozzi, J. Chem. Phys. 25, 1024 (1956).
- [13] J. C. Phillips, Bonds and Bands in Semiconductors, Academic Press, New York 1973.
- [14] A. Zaoui, M. Ferhat, B. Khelifa, J. P. Dufour, and H. Aourag, Phys. Status Solidi (b) 185, 163 (1994).
- [15] M. Ferhat, A. Zaoui, M. Certier, and B. Khelifa, Phys. Status Solidi (b) 195, 415 (1996).
- [16] M. Fuchs, J. L. F. Da Silva, C. Stampfl, J. Neugebauer, and M. Scheffler, Phys. Rev. B 65, 245212 (2002).
- [17] L. E. Ramos, L. K. Teles, L. M. R. Scolfaro, J. L. P. Castineira, A. L. Rosa, and J. R. Leite, Phys. Rev. B 63, 165210 (2001).
- [18] A. Zoroddu, F. Bernardini, P. Ruggerone, and V. Fiorentini, Phys. Rev. B 64, 045208 (2001).
- [19] S. P. Lepkowski, J. A. Majewski, and G. Jurczak, Phys. Rev. B 72, 245201 (2005).
- [20] V. R. Saunders, R. Dovesi, C. Roetti, R. Orlando, C. M. Zicovich-Wilson, N. M. Harrison, K. Doll, B. Civalleri, I. J. Bush, Ph. D'Arco, and M. Llunell, CRYS-TAL2003 User's Manual, University of Torino, Torino 2003.
- [21] C. Pisani and R. Dovesi, Int. J. Quantum Chem. 17, 501 (1980).
- [22] M. D. Towler, A. Zupan, and M. Causa, Comp. Phys. Commun. 98, 181 (1996).
- [23] F. Biggs, L. B. Mandelsohn, and J. B. Mann, At. Data Nucl. Data Tables 16, 201 (1975).
- [24] S. Hosoya, T. Fukamachi, and M. Shimazu, J. Phys. Soc. Jpn. 30, 202 (1971).
- [25] B. K. Sharma, A. Gupta, H. Singh, S. Perkkiő,

- A. Kshirsagar, and D.G. Kanhere, Phys. Rev. B **37**, 6821 (1988).
- [26] D. N. Timms, Compton Scattering Studies of Spin and Momentum Densities, PhD Thesis, University of Warwick, England 1989.
- [27] J. P. Perdew and A. Zunger, Phys. Rev. B 23, 5048 (1981).
- [28] A. D. Becke, Phys. Rev. A 38, 3098 (1988).
- [29] J. P. Perdew and Y. Wang, Phys. Rev. B 33, 8800 (1986); J. P. Perdew and Y. Wang, Phys. Rev. B 45, 13244 (1992).
- [30] P. M. W. Gill, B. G. Johnson, J. A. Pople, and M. J. Frisch, Chem. Phys. Lett. 197, 499 (1992); B. G. Johnson, P. M. W. Gill, and J. A. Pople, J. Chem. Phys. 98, 5612 (1993); J. Muscat and C. Klauber, Surf. Sci. 491, 226 (2001).
- [31] S. H. Vosko, L. Wilk, and M. Nusair, Can. J. Phys. 58, 1200 (1980).
- [32] C. Lee, W. Yang, and R. G. Parr, Phys. Rev. B 37, 785 (1988).
- [33] A. D. Becke, in: Challenge of d and f Electrons: Theory and Computation (Eds. D. R. Salahub, M. C. Zerner), American Chemical Society, Washington DC 1989, Chapter 12, pp. 165.
- [34] http://www.crystal.unito.it/Basis_sets/aliminium.html; http://www.crystal.unito.it/Basis_sets/nitrogen.html.
- [35] D. R. Lide (Ed.), Handbook of Chemistry and Physics, CRC Press, New York 2001.
- [36] A. Rubio, J. L. Corkill, M. L. Cohen, E. L. Shirley, and S. G. Louie, Phys. Rev. B 48, 11810 (1993).
- [37] M. G. M. Armenta, A. Reyes-Serrato, and M. A. Borja, Phys. Rev. B 62, 4890 (2000).
- [38] C. Stampfl and C. G. Van de Walle, Phys. Rev. B 59, 5521 (1999).
- [39] L. I. Berger, Semiconductor Materials, CRC Press, New York 1997.
- [40] W. Y. Ching and B. N. Harmon, Phys. Rev. B 34, 5305 (1986).
- [41] I. N. Remediakis and E. Kaxiras, Phys. Rev. B 59, 5536 (1999).
- [42] N. L. Heda, S. Mathur, B. L. Ahuja, and B. K. Sharma, Phys. Status Solidi (b) 244, 1070 (2006); B. L. Ahuja and N. L. Heda, Z. Naturforsch. 61a, 364 (2006); B. L. Ahuja and N. L. Heda, Radiat. Phys. Chem. 76, 921 (2007)
- [43] B. L. Ahuja, S. Khera, S. Mathur, and N. L. Heda, Phys. Status Solidi (b) 243, 625 (2006).